Comparative Analysis of Small-Signal Dynamics in Virtual Synchronous Machines and Frequency-Derivative-Based Inertia Emulation

[*,†]Jon Are Suul

*SINTEF Energy Research
7465 Trondheim, Norway
Jon.A.Suul@sintef.no, salvatore.darco@sintef.no

[*]Salvatore D'Arco

[†]Department of Engineering Cybernetics
Norwegian University of Science and Technology
7495 Trondheim, Norway

***Abstract*—This paper presents a comparison of small-signal dynamics for a current controlled Virtual Synchronous Machine (VSM), a voltage controlled VSM and a *df/dt*-based control strategy for inertia emulation. The comparison is based on state-space models of the considered control schemes, which are linearized and utilized for eigenvalue-based analysis. Starting from a comparison of the three schemes with manually tuned controller parameters, it is shown that the current controlled VSM can be unstable for strong grid conditions, while the df/dt-based control becomes unstable when the grid impedance is high. Thus, an iterative tuning algorithm based on eigenvalue parametric sensitivities is applied to investigate how much the time-response and damping of the critical modes can be improved. Limitations to the dynamic performance are identified by participation factor analysis of the critical modes. The results demonstrate that all the investigated schemes can be stable for a wide range of operating conditions, but with inherent differences in the inertial response.**

***Index Terms*—Eigenvalues, Linearization, State-Space Models, Virtual Inertia, Virtual Synchronous Machines.**

I. Introduction

Large-scale integration of new generation sources with power electronic grid interfaces and corresponding decommissioning of traditional generation plants with synchronous generators is expected to cause a reduction of the equivalent inertia in power systems [1], [2]. To compensate for reduced rotating masses connected directly to the grid by electrical machines, power electronic converters can be controlled to provide virtual inertia. Various control strategies for inertia emulation have been proposed for a wide range of applications, including distributed generation sources, energy storage systems, STATCOMs and HVDC transmission schemes [3]-[8]. Especially HVDC converter stations have to the potential to provide significant contributions to the equivalent inertia due to the high power ratings. Thus, recent studies have proposed and analyzed various approaches for providing virtual inertia from HVDC systems [9]-[13].

This work was supported by the project "HVDC Inertia Provision" (HVDC Pro), financed by the ENERGIX program of the Research Council of Norway (RCN) with project number 268053/E20 and the industry partners; Statnett, Statoil, RTE and ELIA.

The general intention with control strategies for providing virtual inertia from power electronic converters is to emulate the electromechanical characteristics of synchronous generators. Thus, several control schemes proposed for this purpose have been referred to as Virtual Synchronous Machines (VISMA or VSMs) [14]-[16], Virtual Synchronous Generators (VSGs) [17]-[20], or Synchronverters [21]. The various schemes generally obtain the emulation of synchronous machine inertia by two different approaches:

i) *Internal simulation of the electromechanical swing equation of a synchronous machine.* This approach ensures a power-balance-based grid synchronization mechanism and provides voltage or current references for controlling the power converter to provide a similar response as a synchronous machine.
ii) *Calculation of the equivalent inertial response of a synchronous machine from the measured derivative of the grid frequency.* The resulting power reference can be used as an additional reference signal for a conventional control scheme of the power electronic converter.

Only implementations with internal simulation of an electromechanical swing equation would be capable of emulating all the operating modes of a synchronous machine, including islanded operation [22]. Thus, in the following, only such schemes are referred to as VSMs. However, these VSM-based control schemes rely on the simulated virtual swing equation for grid synchronization and power flow control, which is not compatible with traditional decoupled control of active and reactive power based on grid synchronization by a Phase Locked Loop (PLL). Approaches for Inertia Emulation based on measurement of the grid frequency derivative (*df/dt IE*) are instead designed for providing an additional reference within a conventional PLL-based control system.

Most of the presented schemes for VSM-based control or *df/dt* IE apply multiple control loops, with several adjustable controller parameters. Thus, manual analytical tuning and analysis of such control schemes is challenging. Moreover, it can be difficult to understand the inherent limitations and constrains for dynamic performance and stability implied by the system configuration. State-space modelling and eigenvalue-based analysis of small-signal dynamics can help

978-1-5386-4198-9/18/$31.00 ©2018 IEEE

to reveal the properties of such systems by studying the participation factors and parametric sensitivities of critical modes in the system [23]. Such techniques have been already applied to analyze individual VSMs and *df/dt* IE schemes, or larger systems with a single applied strategy for inertia emulation [9], [12], [13], [15], [16]. However, it is still an open issue to identify what is the most suitable approach for providing virtual inertia with desirable dynamic characteristics over a wide range of operating conditions.

In this paper, the small-signal dynamics of two different VSM-based control schemes and one example of a *df/dt* IE scheme are compared by analyzing the eigenvalues, participation factors and parametric sensitivities of small-signal state-space models representing each scheme. The three schemes are first analyzed with controller parameters selected by conventional tuning rules or simulation-based trial-and-error procedures. It is subsequently evaluated how the system dynamics are influenced by large variations in the grid impedance. Then, an iterative tuning algorithm based on eigenvalue parametric sensitivity, as presented in [24], is applied to all the three schemes. The algorithm is utilized to adjust a subset of the controller parameters with the objective of obtaining the fastest possible response of the slowest mode in each case. The participation factors and sensitivities of the slowest mode resulting after applying the algorithm are discussed to identify the main properties limiting the dynamics and stability margins of each case. The results demonstrate that all the three investigated schemes can be tuned to ensure acceptable stability margins. The voltage controlled VSM can obtain the fastest and most damped response, but compared to the other schemes this limits the capability for providing fast inertial response during frequency variations.

II. Modelling and Simulation of Investigated Approaches for Providing Virtual Inertia

In the following, the three assumed control schemes, and their corresponding models when connected to an ideal grid equivalent, are briefly presented. As a point of reference and for verification of results from small-signal eigenvalue analysis, the three schemes are simulated in Matlab/Simulink/SimPowerSystems. Non-linear state-space models of the cases are also established on the general form:

$$\dot{\mathbf{x}} = f\left(\mathbf{x}, \mathbf{u}\right) \tag{1}$$

These analytical models will be used to obtain linearized small-signal state-space models, and for calculating the steady-state operating points for linearization of the system. For the figures and equations presented in the following, upper case symbols indicate variables and parameters in physical quantities, while lower case symbols represent per unit quantities. Bold symbols represent variables expressed on complex space vector form as $\mathbf{x} = x_d + jx_q$. The applied per unit system is based on the rated apparent power of the converter and the peak value of the rated phase voltage, and is used for all analysis and presentation of results.

A. Current-Controlled Virtual Synchronous Machine

The first scheme is a VSM where a simulated synchronous machine model provides current references for a conventional set of decoupled PI current controllers in a synchronous

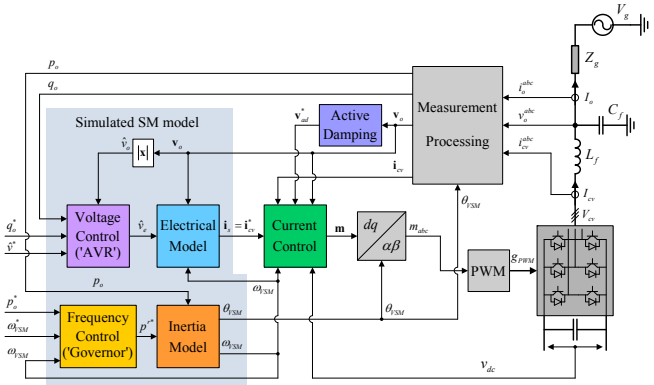

Fig. 1. Overview of control structure for current controlled VSM with quasi-stationary electrical model (QSEM) [16]

reference frame established by the VSM swing equation. A quasi-stationary equation is used to represent the impedance of the simulated synchronous machine, as proposed in [20]. Thus, this scheme is referred to as a Current Controlled VSM (CCVSM) with Quasi-Stationary Electrical Model (QSEM).

An overview of the control system and the assumed electrical configuration with a simplified grid equivalent is shown in Fig. 1. A non-linear state-space model of the overall system is documented in detail in [16]. It should be noted that the QSEM representation of the simulated synchronous machines implies that the current references $\mathbf{i}^*_{cv}$ for the converter correspond to the stator currents $\mathbf{i}_s$ of the emulated synchronous machine. These current references are calculated directly from the voltage amplitude reference $\hat{v}_e$ provided by the voltage controller according to:

$$\mathbf{i}^*_{cv} = \mathbf{i}^{QSEM}_s = \frac{\hat{v}_e - \mathbf{v}_m}{\left(r_s + j \cdot \omega_{VSM} l_s\right)} \tag{2}$$

In this equation, r_s and l_s represent the equivalent resistance and inductance of the emulated synchronous machine, $\hat{v}_e$ is the internal voltage behind this virtual impedance, and $\mathbf{v}_m$ represents the low-pass filtered d- and q-axis components of the measured voltage $\mathbf{v}_o$.

The virtual swing equation of the VSM is given by:

$$\frac{d\omega_{VSM}}{dt} = \frac{p^*_o}{T_a} - \frac{p_o}{T_a} - \frac{k_d\left(\omega_{VSM} - \tilde{\omega}_g\right)}{T_a} - \frac{k_\omega\left(\omega_{VSM} - \omega^*\right)}{T_a} \tag{3}$$

where $\tilde{\omega}_g$ is the estimated grid frequency needed for implementing the damping term. In this case, the grid frequency is estimated internally within the virtual swing equation by applying a low-pass filter with crossover frequency ω_d to the VSM speed ω_{VSM} [16]. A power-frequency droop, corresponding to an idealized governor function with a droop gain of k_ω, is also included in (3). For practical implementation, the phase angle θ_{VSM}, which is used for the *dq*-transformations of the control system, is obtained directly by integration of ω_{VSM}. However, for the modelling of the system, only the phase angle displacement between the VSM reference frame and the grid voltage should be represented. The corresponding state equation is defined as:

$$\frac{d\delta\theta_{VSM}}{dt} = \omega_{VSM} \cdot \omega_b - \omega_g \cdot \omega_b \tag{4}$$

The non-linear state-space model of the QSEM-based CCVSM from [16], is expressed on the form given by (1),

This is the accepted version of a paper published in Proceedings - 2018 IEEE 18th International Conference on Power Electronics and Motion Control - PEMC.
DOI: 10.1109/EPEPEMC.2018.8522010

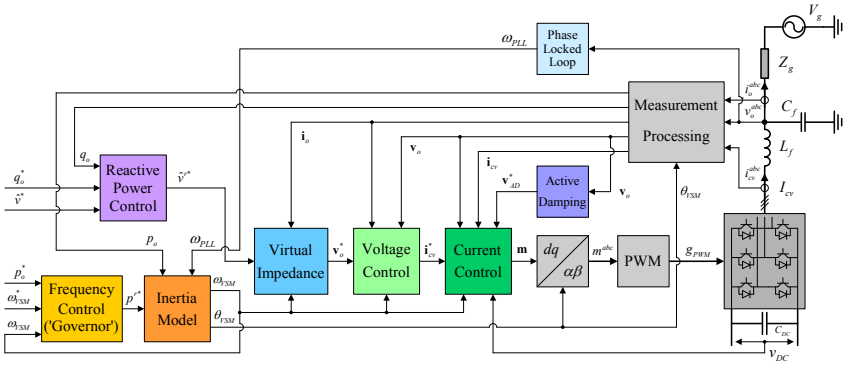

Fig. 2. Overview of control structure for voltage controlled VSM [15]

with the state vector $\mathbf{x}_{CCVSM}$ and the input vector $\mathbf{u}_{CCVSM}$ defined by (5).

$$\mathbf{x}_{CCVSM} = \left[v_{o,d} \quad v_{o,q} \quad i_{cv,d} \quad i_{cv,q} \quad \gamma_d \quad \gamma_q \quad i_{o,d} \quad i_{o,q} \ldots \right.$$
$$\left. \ldots \varphi_d \quad \varphi_q \quad \xi \quad q_m \quad \omega_{VSM} \quad \delta\theta_{VSM} \quad \kappa \quad v_{m,d} \quad v_{m,q} \right]^T \quad (5)$$
$$\mathbf{u}_{CCVSM} = \left[p_0^* \quad q_0^* \quad \hat{v}_g \quad \hat{v}^* \quad \omega^* \quad \omega_g \right]^T$$

In addition to the variables already defined in Fig. 1 or explained for (2)-(4), $\gamma_{d,q}$ represent integrator states of the current controllers, and $\varphi_{d,q}$ represent states utilized for active damping of LC resonances. Furthermore, ξ represents the integrator state of the voltage controller, q_m is the state of a low pass filer on the reactive power measurement, and κ represents the state of the low pass filter used for estimating the grid frequency. Based on the resulting non-linear state-space model documented in [16], a small-signal model can be generated for any feasible operating point of the CCVSM.

B. *Voltage-Controlled Virtual Synchronous Machine*

As the second case, a voltage controlled VSM (VCVSM) is analyzed. Thus, a closed loop *dq* voltage controller provides the current references to the inner loop current controller. An overview of the control system is shown in Fig. 2, and further descriptions as well as documentation of the state-space model of this scheme are available in [15].

Compared to the CCVSM described in the previous section, it should be noted that the applied VCVSM is utilizing a Phase Locked Loop (PLL) for estimating the grid frequency in the virtual swing equation. Furthermore, the internal voltage amplitude reference $\hat{v}^{r*}$ is provided by a simple reactive power droop [15]. The voltage reference for the closed loop voltage controller is resulting from $\hat{v}^{r*}$ and the voltage drop on a quasi-stationary virtual impedance as:

$$\mathbf{v}_o^* = \hat{v}^{r*} - \left(r_v + j \cdot \omega_{VSM} \cdot l_v \right) \cdot \mathbf{i}_o \quad (6)$$

The state-space model of the VCVSM, is defined by the state vector $\mathbf{x}_{VCVSM}$ and the input vector $\mathbf{u}_{VCVSM}$ given by:

$$\mathbf{x}_{VCVSM} = \left[v_{o,d} \quad v_{o,q} \quad i_{cv,d} \quad i_{cv,q} \quad \gamma_d \quad \gamma_q \quad i_{o,d} \quad i_{o,q} \quad \varphi_d \quad \varphi_q \ldots \right.$$
$$\left. \ldots v_{PLL,d} \quad v_{PLL,q} \quad \varepsilon_{PLL} \quad \delta\theta_{VSM} \quad \xi_d \quad \xi_q \quad q_m \quad \delta\omega_{VSM} \quad \delta\theta_{PLL} \right]^T \quad (7)$$
$$\mathbf{u}_{VCVSM} = \left[p_0^* \quad q_0^* \quad \hat{v}_g \quad \hat{v}^* \quad \omega^* \quad \omega_g \right]^T$$

The state variables and inputs are the same as for the CCVSM, except from $\mathbf{v}_{PLL}$ and ε_{PLL}, which are internal states of the PLL, and $\xi_{d,q}$ which represent the integrator states of the *dq* voltage controller.

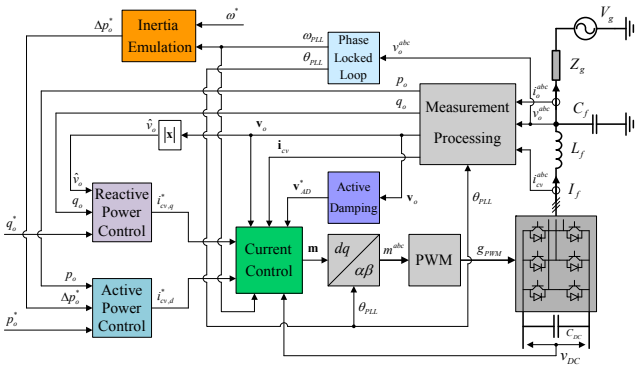

Fig. 3. Overview of df/dt-based inertia emulation strategy providing an additional power reference to a conventional control system

C. *Conventional Control with df/dt Inertia Emulation*

A general scheme for *df/dt* IE has also been studied for comparison of small-signal dynamics with respect to the presented VSM-based schemes. An overview of the assumed control system is shown in Fig. 3. It can be seen from the figure that this scheme relies on a conventional PLL-based control structure with inner loop current controllers and closed loop control of active and reactive power. Thus, the inertia emulation is providing the additional power reference Δp_o^* to the power controller. This structure is studied since it allows for inertia emulation by acting on the references for an outer loop controller of a conventional control system, without requiring modifications of the conventional control loops or the PLL-based grid synchronization strategy. Since the inertia emulation is provided by an outer loop power reference, this control scheme could be assumed to provide the slowest approach for *df/dt*-based inertia emulation. A faster *df/dt*-based inertia emulation could for instance be achieved by acting directly on the current references [5], [25]

For *df/dt*-based inertia emulation, it should also be considered that implementation of a pure derivative function can amplify noise in the control system. Thus, a limited derivative is preferred, and the power reference resulting from the inertia emulation with a frequency droop can be calculated from the grid frequency estimated by the PLL as [13]:

$$\Delta p_o^*(s) = -k_J \frac{s\omega_{LPf}}{s + \omega_{LPf}} \omega_{PLL}(s) + k_\omega \left(\omega^* - \omega_{PLL}(s) \right) \quad (8)$$

In this equation, k_J is the constant associated with the equivalent inertia, and k_ω is the same droop gain constant as

This is the accepted version of a paper published in Proceedings - 2018 IEEE 18th International Conference on Power Electronics and Motion Control - PEMC.
DOI: 10.1109/EPEPEMC.2018.8522010

TABLE I COMMON PARAMETERS FOR THE THREE SCHEMES

Parameter	Value	Parameter	Value
Rated voltage $V_{N,LL,RMS}$	380kV	Filter inductance l_1	0.15 pu
Rated power S_b	1.2 GVA	Filter resistance r_{L1}	0.003 pu
Rated angular frequency ω_b	2π*50 Hz	Filter capacitance c_f	0.09 pu
Current controller gain: k_{pc}, k_{ic}	2.39, 15	Grid side inductance l_g	0.20 pu
Active damping, k_{ad}, $\omega_{LP,ad}$	1.5 20 rad/s	Grid side equivalent series resistance r_g	0.001 pu
PLL voltage filter crossover frequency, $\omega_{LP,PLL}$	500 rad/s	PLL controller gains, $k_{p,PLL}$, $k_{i,PLL}$	0.084, 4.69
Frequency reference, ω^*	1.0 pu	Reactive power droop gains, k_q (= $1/k_v$)	0.1 pu
Frequency droop gain, k_ω	20 pu	Voltage reference $\hat{v}^*$	1.0 pu

used in the VSM schemes. The limited derivative of the grid frequency is obtained as the difference between the estimated frequency from the PLL and a low-pass filtered version of the same signal, where the crossover frequency of the low-pass filter is defined by $\omega_{LP\omega}$. Thus, the calculation of the power reference from the inertia emulation according to (8) can be easily expressed on state-space form.

The resulting non-linear state-space model of the system in Fig. 3 is expressed on the form given by (1), with the state vector $\mathbf{x}_{df/dt}$ and the input vector $\mathbf{u}_{df/dt}$ defined by:

$$\mathbf{x}_{df/dt} = \begin{bmatrix} v_{o,d} & v_{o,q} & i_{cv,d} & i_{cv,q} & \gamma_d & \gamma_q & i_{o,d} & i_{o,q} & \varphi_d & \varphi_q \dots \\ \dots v_{PLL,d} & v_{PLL,q} & \varepsilon_{PLL} & \delta\theta_{PLL} & \rho & p_m & \sigma & q_m & \hat{v}_{om} & \omega_{LP\omega} \end{bmatrix}^T \quad (9)$$

$$\mathbf{u}_{df/dt} = \begin{bmatrix} p_0^* & q_0^* & \hat{v}_g & \hat{v}^* & \omega^* & \omega_g \end{bmatrix}^T$$

A detailed documentation of the modelling of the inner control loops and the PLL is available in [26], and most of the variables in this model have been already defined for the VSM schemes. However, outer loop PI controllers for the active and reactive power, with low-pass filters in the feedback signals are included in the model. Thus, the state ρ represents the integrator of the active power controller, p_m and q_m represent the low pass filters on the power measurements, σ represents the integrator of the reactive power controller and $\hat{v}_{om}$ represents a low pass filter on the voltage amplitude used for implementing a voltage droop in the reactive power controller.

III. COMPARATIVE ANALYSIS OF SMALL-SIGNAL DYNAMICS

For analyzing the small signal dynamics of the three control schemes presented in section II, the corresponding state-space models are linearized at an operating point specified by the input signals and expressed as:

$$\Delta\dot{\mathbf{x}} = \mathbf{A}(\mathbf{x}_0)\cdot\Delta\mathbf{x} + \mathbf{B}(\mathbf{x}_0)\cdot\Delta\mathbf{u} \quad (10)$$

Eigenvalue-based analysis is then applied to study the characteristics of the small-signal dynamics for the three schemes with parameters and input signals as defined in Table I and Table II. It should be noted that all three cases are studied for connection to an ideal equivalent grid model with the frequency provided as an input variable. Thus, only the response of the local control system is considered, without attempting to assess dynamic interactions with the physical inertia of traditional generation plants.

TABLE II PARAMETERS WITH SPECIFIC VALUES FOR EACH SCHEME

Parameter	Value	Parameter	Value
VSM Inertia constant T_a	2 s	Power controller gains for *df/dt* IE, $k_{p,pac}$, $k_{i,pac}$	2, 50
VSM Damping constant k_d	50	Active power measurement filter for *df/dt* IE, ω_{pac}	50 rad/s
CCVSM LP crossover frequency for grid frequency estimation ω_a	10 rad/s	Reactive power controller gains for *df/dt* IE, $k_{p,qac}$, $k_{i,qac}$	1.0, 1.0
CCVSM voltage filter crossover frequency ω_{vo}	10 rad/s	Reactive power filter for *df/d IE* ω_{qac}	50 rad/s
CCVSM voltage controller gain, k_{pv}, k_{iv}	1, 20	Voltage amplitude filter, *df/dt* IE, ω_{voa}	10 rad/s
VCVSM dq voltage controller gain, k_{pv}, k_{iv}	0.7, 895	Frequency filter for *df/dt* IE, $\omega_{LP,\omega}$	6.3 rad/s
Virtual Impedance l_v, = l_s, r_v = r_s	0.2, 0.01 pu	Frequency derivative gain for *df/dt* IE, k_J	80

A. Analysis of Critical Modes of the Three Control Schemes

As a starting point, the slowest modes for all the three schemes, with real part of the eigenvalues higher than −20 or damping ratio ζ lower than 8%, are listed in Table III. The main participating states in each mode are also listed in the table, in descending order according to the absolute value of the participation factor. Furthermore, the table includes a list of the parameters with the highest parameter sensitivity along the real axis for each analyzed mode. The real part of the sensitivity $\alpha_{n,k}$ of the eigenvalue λ_n with respect to the parameter ρ_k is calculated as:

$$\mathrm{Re}(\alpha_{n,k}) = \mathrm{Re}\left(\frac{\partial\lambda_n}{\partial\rho_k}\right) = \mathrm{Re}\left(\frac{\boldsymbol{\Phi}_n^T\frac{\partial\mathbf{A}}{\partial\rho_k}\boldsymbol{\Psi}_n}{\boldsymbol{\Phi}_n^T\boldsymbol{\Psi}_n}\right) \quad (11)$$

where $\boldsymbol{\Psi}_n$ and $\boldsymbol{\Phi}_n$ are the left and right eigenvectors associated with λ_n. In Table III, the parameters are listed in descending order according to the absolute value of (11), and the direction of the sensitivity is indicated by a negative sign (−) in front of parameters for which an increase of the value will reduce the real part of the corresponding eigenvalue.

From the results collected in Table III, it can be noticed that the CCVSM has two critical oscillatory modes $\lambda_{1,2}$ and $\lambda_{8,9}$. The mode $\lambda_{1,2}$ with low oscillation frequency is clearly associated with the inertial dynamics of the VSM, since it has high participation from the states $\delta\theta_{VSM}$, κ and ω_{VSM}. However, the mode is also associated with the low pass filtering of the measured q-axis voltage, by the state v_{omq}. The parametric sensitivities also show how this mode is sensitive to the virtual impedance parameters l_s, and r_s, as well as the inertia time constant T_a, and the crossover frequencies ω_{vo} and ω_d. These low pass filters are used for filtering the voltage measurement as part of the current reference calculation and for the estimation of the grid frequency in the damping of the virtual swing equation, respectively. The mode $\lambda_{8,9}$ is instead mainly associated with the voltages and currents in the electrical circuit, and represent a LC-oscillation related to the output filter. However, it should be noticed that the parametric sensitivities reveal that $\lambda_{8,9}$ is most sensitive to the virtual impedance parameters l_s, and r_s. This demonstrates that the CCVSM with a quasi-stationary electrical model implies a relatively strong coupling between the simulated electrical model of the VSM and the parameters of the electrical system.

This is the accepted version of a paper published in Proceedings - 2018 IEEE 18th International Conference on Power Electronics and Motion Control - PEMC.
DOI: 10.1109/EPEPEMC.2018.8522010

From the results listed in Table III, it can also be observed that the VCVSM does not have any critical eigenvalue with respect to stability for the parameters and operating conditions according to Table I and Table II. Indeed, the two slowest modes for this case are eigenvalues with only real parts, and they are mainly associated with the inner loop current controllers.

The case with *df/dt* IE has two critical complex conjugate eigenvalues, $\lambda_{1,2}$ and $\lambda_{6,7}$. The results in Table III show that the mode $\lambda_{1,2}$ with high oscillation frequency is associated with the *q*-axis voltage filtering in the PLL and with the electrical states of the system. Thus, the highest parameter sensitivity appears for the PLL gain as well as the gains of the current controllers and the active damping of LC oscillations. However, the mode $\lambda_{6,7}$ is characterized by long settling time and low oscillation frequency. This mode is mainly associated with the bandwidth of the PLL and the estimation of the frequency derivative, as determined by the internal low pass filter state $\omega_{PLL,f}$ and the estimated phase angle displacement $\delta\theta_{PLL}$ with respect to the grid voltage. The mode $\lambda_{6,7}$ also has participation from the states ρ and p_{acm} associated with the integrator and the low pass filter of the active power feedback, as well as from the integrator state ε_{PLL} of the PI controller of the PLL. Thus, this mode is mainly sensitive to the parameters of the PLL and the active power controller. It should also be noted that the *df/dt* IE has a very slow eigenvalue with a purely real value of −0.51, which is associated with the reactive power controller. Thus, this eigenvalue can be expected to limit the minimum settling time of the system.

TABLE III IDENTIFIED CRITICAL MODES WITH CORRESPONDING PARTICIPATING STATES AND DOMINANT PARAMETER SENSITIVITIES

	Modes with Re(λ) > −20 or ζ <8 %		**Main participating states (>0.05)**	**Parameter sensitivities (max 5 and >.2)**
CCVSM	$\boldsymbol{\lambda_{1,2}}$	$\boldsymbol{-1.78 \pm j\ 10.80}$	$\delta\theta_{VSM}$, v_{omq}, κ, ω_{VSM}	l_s, $-r_s$, T_a, $-\omega_{vo}$, ω_{df}
	λ_3	-13.74	κ, v_{omq}, $\delta\theta_{VSM}$	l_s, $-r_s$, $-\omega_{df}$, $-\omega_{vo}$, T_a
	λ_4	-17.91	κ, φ_q, φ_d, $\delta\theta_{VSM}$, v_{omd}, ξ, ω_{VSM}	l_s, r_s, $k_{p,v}$, $-k_{ffe}$, $-k_q$
	λ_5	-6.02	ξ, γ_q, v_{omd}, γ_d	$-k_q$, l_s, $k_{p,c}$, $-r_s$, $k_{p,v}$
	$\lambda_{6,7}$	$-6.33 \pm j\ 0.15$	γ_d, γ_q, ξ, v_{omd}	$k_{p,c}$, $-k_q$, r_s, l_s, $-k_{i,c}$
	$\boldsymbol{\lambda_{8,9}}$	$\boldsymbol{-208.6 \pm j2962}$	v_{oq}, v_{od} i_{oq} i_{cvd} i_{od} i_{cvq}	$-r_s$, $-l_s$, $-k_{ad}$, k_{ffv}, k_{pv}
VCVSM	$\lambda_{1,2}$	$-19.52 \pm j27.20$	ε_{PLL}, $\delta\omega_{VSM}$, $\delta\theta_{PLL}$, $\delta\theta_{VSM}$, v_{PLLq}	$-k_{p,PLL}$, l_v, $-r_v$, t_a, $k_{i,PLL}$
	$\lambda_{3,4}$	$-10.52 \pm j20.54$	$\delta\theta_{VSM}$, $\delta\theta_{PLL}$, $\delta\omega_{VSM}$, ε_{PLL}	$-l_v$, $k_{p,PLL}$, r_v, t_a, $-k_{i,PLL}$
	λ_5	-6.29	γ_q	k_{pc}, $-k_{ic}$
	λ_6	-6.29	γ_d	k_{pc}, $-k_{ic}$
df/dt IE	$\boldsymbol{\lambda_{1,2}}$	$\boldsymbol{-16.04 \pm j1402}$	v_{PLLq}, $i_{o,d}$, $i_{o,q}$, $v_{o,d}$, $v_{o,q}$, $i_{cv,q}$, $i_{cv,d}$	$k_{p,PLL}$, $k_{p,pac}$, $k_{p,c}$, k_{ffv}, $-k_{ad}$
	$\lambda_{3,4}$	$-19.99 \pm j1.45$	φ_q, φ_d, ρ, ε_{PLL}	$-\omega_{ad}$, $k_{p,PLL}$
	$\boldsymbol{\lambda_5}$	$\boldsymbol{-0.51}$	σ	$-k_{i,qac}$, $k_{p,qac}$
	$\lambda_{6,7}$	$-8.92 \pm j4.97$	ω_{PLLf}, $\delta\theta_{PLL}$, ρ, p_{acm}, ε_{PLL}	$-k_{p,PLL}$, k_{ppac}, $-\omega_{lpJ}$
	λ_8	-10.09	v_{oAm}	$-\omega_{voa}$, $-k_{drpq}$
	λ_9	-6.28	γ_q, γ_d, $\omega_{LP\omega}$	k_{pc}, ω_{lpJ}, $-k_{i,c}$
	λ_{10}	-6.28	ω_{PLLf}	$-\omega_{lpJ}$

B. *Variations of grid impedance*

For further assessing and comparing how the different schemes respond to parameter variations, Fig. 4 shows the eigenvalue trajectories when the grid inductance l_g is changed in the range from 0.05 pu (SCR ≈20 – indicated by blue color) to 0.5 pu (SCR ≈2 – indicated by red color). In these figures, all eigenvalues are marked with black triangles for cases when the system is unstable. As shown in Fig. 4 a), the CCVSM experiences instability due to the mode given by $\lambda_{8,9}$ for low values of the grid inductance. The mode $\lambda_{1,2}$ also has very low damping in these conditions. However, this scheme is robust with respect to operation with high grid inductance values, corresponding to weak grid conditions.

The VCVSM is stable for the full range of considered parameters variations and no potential instabilities are identified within reasonable parametric variations of the electrical system. However, it should be noted that this scheme can be difficult to tune, especially in case of low switching frequency limiting the bandwidth of the inner loop current controllers [24]. Still, the results show that when this scheme is properly tuned, it can ensure good performance with respect to small-signal stability. Indeed, it can be seen in Fig. 4 b) that the slowest eigenvalues of the VCVSM are not influenced by the variations in the grid side inductance, and that no other eigenvalues are reaching a higher real value due to this range of parameter variations.

For the *df/dt* IE, Fig. 4 c) shows that stability problems associated with mode $\lambda_{1,2}$ appears for weak grid conditions with high values of grid inductance. The damping of mode $\lambda_{6,7}$ is also reduced and the settling time is increasing with higher grid inductance values. These limitations should be expected, since the *df/dt* IE depends on the PLL for estimating the grid frequency derivative, and weak grid conditions are known to cause stability problems due to interactions between the PLL and other control loops [27]. However, the measurement of the frequency derivative and the transient power injection due to the inertia emulation are aggravating this effect. Thus, very weak grid conditions with SCR below 2 are not considered in this context, since stable operation under such conditions could be expected to require retuning or redesign of the PLL. Beyond the two complex conjugate modes that are influenced by the grid inductance, it can be noticed that the slowest real pole of the system is not much influenced by grid inductance variations.

IV. ITERATIVE TUNING FOR STABILITY ENFORCEMENT AND IMPROVEMENT OF DYNAMIC PERFORMANCE

To study how a robust performance of all the three investigated schemes can be achieved over a wide range of system parameters, the tuning of the control systems has been reconsidered by applying the iterative sensitivity-based tuning algorithm proposed in [24]. This algorithm automatically identifies the eigenvalue with the highest real part and utilizes the parametric sensitivity according to (11) for identifying and modifying the parameter that has the highest influence on the real part of the eigenvalue. The algorithm can operate on a sub-set of the system parameters, so that the iterative operation for gradually moving the system eigenvalues towards the left is only allowed to change the freely tunable controller parameters. In the following, only the parameters of the outer loop controllers are selected as tunable parameters

This is the accepted version of a paper published in Proceedings - 2018 IEEE 18th International Conference on Power Electronics and Motion Control - PEMC.
DOI: 10.1109/EPEPEMC.2018.8522010

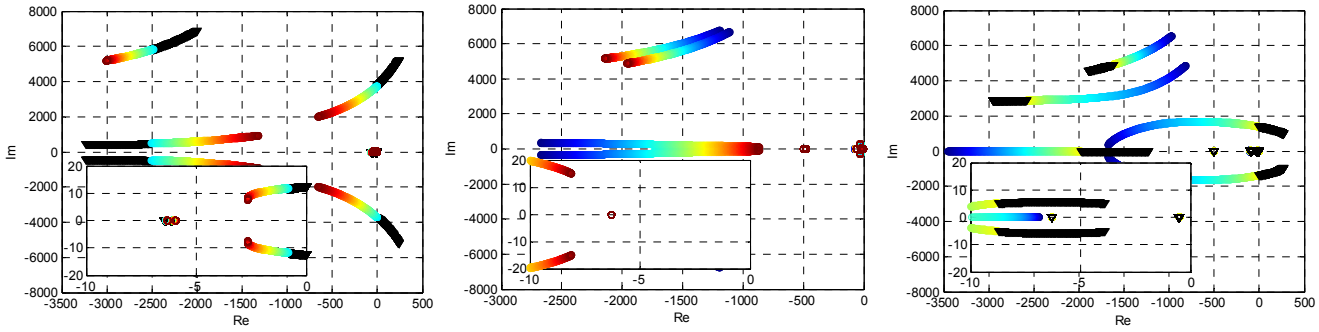

a) CCVSM b) VCVSM c) df/dt IE

Fig. 4. Eigenvalue trajectory for change of grid inductance from l_g = 0.05 pu (blue) to l_g = 0.5 pu (red)

for the applied algorithm. Thus, no parameters related to the electrical circuit or the current controllers will be modified. The inertia time constant T_a is also kept constant, since it is assumed that this value will be specified according to a requirement for providing virtual inertia.

A. Results from Iterative Tuning Algorithm

The results from applying the sensitivity-based tuning algorithm from [24] are presented in Fig. 5 for all the three investigated schemes. For the CCVSM, the iterative tuning algorithm is applied for the case of l_g = 0.05, since this was the worst investigated case with respect to stability as shown in Fig. 4 a). The resulting trajectory of the eigenvalues are shown in the upper part of Fig. 5 a), while the parameters that are modified by the algorithm are shown in the lower part. It can be noticed that the algorithm is first increasing the virtual inductance l_s, which forces the unstable eigenvalues towards the left. Subsequently, the algorithm modifies the crossover frequency of the low pass filtering of the voltage measurements, ω_{oa}. After changing these parameters, the instability of the system due to the mode $\lambda_{8,9}$ from Table III is avoided. Thus, the algorithm is value of l_s is reduced towards the initial value, to reduce the settling time of mode $\lambda_{1,2}$. The algorithm also changes the power-frequency droop gain k_ω and the crossover frequency ω_d for the damping in the virtual swing equation. As a result, stability is enforced for operation with low values of l_g, and the settling time of the system is decreased for the full range of values assumed for the grid inductance. It can be verified that the parameters resulting from the sensitivity-based iterative re-tuning of the system ensure stability within the full range of considered grid inductance values.

The iterative tuning algorithm has also been applied to the the VCVSM, for the highest grid inductance of l_g = 0.5 pu. In this case, the algorithm is not allowed to change any of the parameters with the highest sensitivity with respect to the slowest pole, as given by Table III. However, for high grid inductance values these slow real eigenvalues have a small sensitivity with respect to the reactive power droop gain. Thus, the algorithm is attempting to move these eigenvalues towards the left by reducing the droop gain k_q. Still, it can be seen from Fig. 5 b) that the slowest eigenvalues do not change much. Indeed, the information regarding these modes in Table III and the fact that the eigenvalues do not change much with the grid inductance already indicated that there were limited possibilities, as well as limited need, for modifying the tuning.

For *df/dt* IE, the iterative tuning algorithm has been also applied with l_g = 0.5 pu, since this case was unstable according to Fig. 4 c). As shown in Fig. 5 c), the iterative tuning algorithm is able to enforce stability of the critical eigenvalue by modifying the gains of the active power controller and the reactive power controller. When stability of the mode $\lambda_{1,2}$ from Table III has been ensured, the algorithm is also trying to reduce the settling time associated with the real eigenvalue λ_5 by reducing the proportional gain k_{pqac} of the reactive power controller. However, this mode cannot be changed much, and it is limited how far towards the left the eigenvalues of the system can be forced. Since this case initially experienced stability problems only for high values of the grid inductance, the controller parameters resulting from the iterative tuning algorithm with l_g = 0.5 are ensuring that the system will be stable with grid inductance below this value.

B. Evaluation of Critical Modes and Time Response After Sensitivity-based Tuning

For verifying the small-signal characteristics of the three different schemes with the controller parameters resulting from the iterative tuning approach, the eigenvalues with the updated parameters have been evaluated for the same conditions as in Table III. The results are presented in Table IV and confirm that the stability characteristics have been improved for the assumed grid inductance value of l_g = 0.2 pu. Indeed, the results for the CCVSM show that the mode $\lambda_{8,9}$ which caused instability with the initial parameters and low grid inductance values is now well damped. Since it has a damping ratio of 0.7 and is not a critical mode anymore, it is marked with grey in the table. The real part of the slowest remaining oscillatory mode $\lambda_{3,4}$, which correspond to $\lambda_{1,2}$ in Table III, has also been reduced. Thus, the settling time of the system has been decreased. This can also be confirmed from the time domain simulation results presented in Fig. 6 a), which shows a faster and more damped response to an ideal step in the grid frequency.

For the VCVSM, it can be noticed that one of the oscillatory modes has become marginally slower due to the retuning of the parameters for a case with high grid inductance. At the same time, the damping has been improved even if the real part of eigenvalue $\lambda_{1,2}$ has been increased. The real part of one of the modes has also been reduced below −20, so that it is not included in Table IV. However, it can be noticed from the simulation results in Fig. 6 b) that the change of parameters and the improved damping of the eigenvalue

This is the accepted version of a paper published in Proceedings - 2018 IEEE 18th International Conference on Power Electronics and Motion Control - PEMC.
DOI: 10.1109/EPEPEMC.2018.8522010

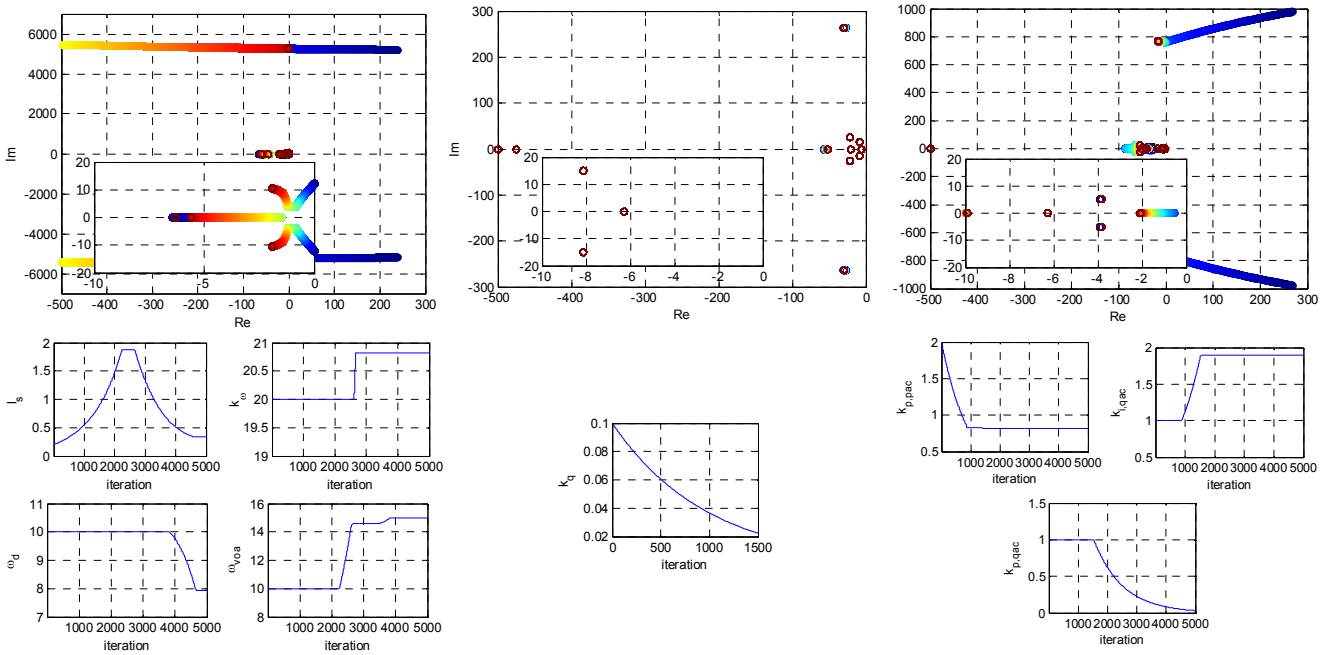

a) CCVSM with l_g = 0.05 pu b) VCVSM with l_g = 0.5 pu c) df/dt IE

Fig. 5. Eigenvalue trajectory and corresponding trace of modifiable parameters when applying sensitivity-based iterative turning for forcing the eigenvalue with the highest real part towards the left

TABLE IV IDENTIFIED CRITICAL MODES AFTER ITERATIVE TUNING, WITH CORRESPONDING PARTICIPATING STATES AND DOMINANT PARAMETER SENSITIVITIES

	Modes with Re(λ) > −20 or ζ <8 %		**Main participating states (>0.05)**	**Parameter sensitivities (max 5 and >.2)**
CCVSM	$\lambda_{1,2}$	$-18.82 \pm j\ 1.66$	φ_d, φ_q, v_{omq}, v_{omd}	l_s, $-r_s$, k_{ad}, $-k_{p,c}$, $-\omega_{ad}$
	$\boldsymbol{\lambda_{3,4}}$	$\mathbf{-2.67 \pm j\ 6.10}$	$\delta\theta_{VSM}$, κ, ω_{VSM}, v_{omq}	l_s, T_a, $-r_s$
	λ_5	-6.00	γ_q, γ_d, ξ, φ_q, φ_d	$k_{p,c}$, $-k_q$, l_s, $-k_{ffv}$, $-k_{i,c}$
	$\lambda_{6,7}$	$-6.63 \pm j\ 0.20$	ξ, γ_d, γ_q, v_{omd}, φ_d, φ_q	$-k_q$, $k_{p,c}$, l_s, $k_{p,v}$, $-k_{ffe}$
	$\lambda_{8,9}$	$-898.0 \pm j\ 838.2$	i_{oq}, i_{od}, v_{oq}, i_{cvd}, v_{od}, v_{omq}, i_{cvq}	r_s, l_s, $-k_{pc}$, k_{ad}, $-k_{ffv}$
VCVSM	$\lambda_{1,2}$	$-8.12 \pm j15.06$	$\delta\theta_{VSM}$, $\delta\theta_{PLL}$, $\delta\omega_{VSM}$, ε_{PLL}	$-l_v$, $k_{p,PLL}$, T_a, r_v, $-k_{i,PLL}$
	λ_3	-6.29	γ_q	k_{pc}, $-k_{ic}$
	λ_4	-6.29	γ_d	k_{pc}, $-k_{ic}$
df/dt	$\lambda_{1,2}$	$\mathbf{-16.22 \pm j767}$	v_{PLLq}, $i_{o,d}$, $i_{o,q}$, $v_{o,d}$, $v_{o,q}$, $i_{cv,q}$	$k_{p,PLL}$, $k_{p,pac}$, $k_{p,c}$, k_{ffv}, $-k_{ad}$
	$\lambda_{3,4}$	$-19.02 \pm j2.49$	φ_d, φ_q, ε_{PLL}, ρ	$k_{p,PLL}$, $-k_{p,qac}$, k_{ad}, $-k_{p,c}$, $-\omega_{ad}$
	λ_5	$\mathbf{-2.11}$	σ	$k_{p,qac}$, $-k_{drpq}$, $-k_{i,qac}$
	$\lambda_{6,7}$	$-3.82 \pm j5.20$	$\delta\theta_{PLL}$, $\omega_{LP\omega}$, p_{acm}, ρ	*NA*
	λ_9	-9.89	v_{oAm}	k_{drpq}, $-\omega_{voa}$, $-k_{p,qac}$
	λ_{10}	-6.28	γ_q, γ_d, $\omega_{LP\omega}$	$k_{p,c}$, ω_{LPJ}, $-k_{i,c}$
	λ_{11}	-6.28	$\omega_{LP\omega}$	$-\omega_{LPJ}$

associated with the inertial dynamics leads to a lower overshoot and smoother response in the active power flow. Thus, the more damped small-signal characteristics are limiting the ability of the control system to provide short-term inertial response to grid frequency variations.

For the *df/dt* IE with l_g = 0.2 pu, the real part of the critical mode $\lambda_{1,2}$ has not changed much with the application of the iterative tuning algorithm. However, the damping is improved, and this mode is now prevented from causing stability problems within the investigated range of grid inductance values. It can also be noted that the slowest real eigenvalue $\lambda_{1,2}$ is slightly more negative than in Table III, indicating that the settling time of the system has decreased. However, the minor changes of the eigenvalues during operation with l_g = 0.2 pu have no significant influence on the time-response of the system as can be seen from Fig. 6 c). Thus, the result of the updated parameters is mainly that the stability range of the system has been improved, while the transient response of the inertia emulation has not been significantly influenced.

V. CONCLUSION

Inertia emulation from power converters is expected to become important in future power systems with a low presence of physical inertia. This paper presented a comparative analysis of the small-signal dynamics of three control schemes intended for providing virtual inertia, a Current Controlled Virtual Synchronous Machine (CCVSM), a Voltage Controlled Virtual Synchronous Machine (VCVSM) and a strategy for frequency-derivative-based Inertia Emulation (*df/dt* IE). The results demonstrate that the three schemes could offer the intended performance over a wide range of operating conditions, if they are properly tuned. However, the *df/dt* IE scheme can be prone to stability problems for high values of grid impedance, while the investigated CCVSM can experience stability problems when operating in strong grids with low inductance. The VCVSM scheme was shown to maintain stable operation over a wide range of grid impedances. Finally, the paper presented the results from applying an iterative tuning procedure based on eigenvalue parametric sensitivity, aiming at enforcing stability and improving the time response of the system by shifting the eigenvalue with the highest real part towards the left in the complex plane. The procedure was shown to prevent stability problems for the *df/dt* IE at high grid inductance values and

This is the accepted version of a paper published in Proceedings - 2018 IEEE 18th International Conference on Power Electronics and Motion Control - PEMC.
DOI: 10.1109/EPEPEMC.2018.8522010

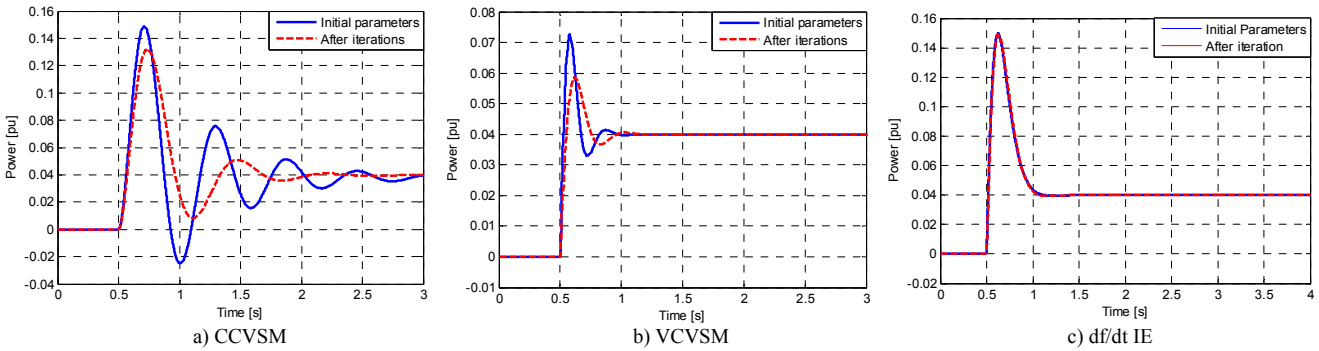

a) CCVSM b) VCVSM c) df/dt IE

Fig. 6. Time domain simulations from Simulink/SimpowerSystems with initial parameters and parameters from sensitivity-based iterative tuning

ensure stability of the CCVSM in strong grids. After re-tuning the controller parameters, reasonable dynamic performance could be ensured for the three schemes over a large range of grid inductance values, with well damped inertial response ensured by the *df/dt* IE and the VCVSM and as slightly more oscillatory response with longer settling time for the CCVSM.

REFERENCES

[1] Y. Wang, V. Silva, M. Lopez-Botet-Zulueta, "Impact of high penetration of variable renewable generation on frequency dynamics in the continental Europe interconnected system," in *IET Renewable Power Generation*, Vol. 10, No. 1, January 2016, pp. 10-16

[2] P. Tielens, D. Van Hertem, "The relevance of inertia in power systems," in *Renewable and Sustainable Energy Reviews*, Vol 55, March 2016, pp. 999-1009

[3] M. Dreidy, H. Mokhils, S. Mekhilef, "Inertia response and frequency control techniques for renewable energy sources: A review," in *Renew. and Sust. Energy Rev.*, Vol 69, March 2017, pp. 144-155

[4] T. Vu Van, J. Diaz, V. Karapanos, A. Woyte, M. Albu, J. Bozelie, T. Loix, D. Federenciuc, "Virtual Synchronous Generator: An Element of Future Grids," in *Proceedings of the IEEE PES Innovative Smart Grid Technologies Conference Europe*, ISGT Europe 2010, Gothenburg, Sweden, 11-13 October 2010, 7 pp.

[5] A. Vassilakis, P. Kotsampopoulos, N. Hatziargyrio, V. Karapanos, "A Battery Energy Storage Based Virtual Synchronous Generator," in *Proceedings of IREP Symposium: Bulk Power System Dynamics and Control – IX Optimization, Security and Control of the Emerging Power Grid*, IREP 2013, Rethymno, Greece, 25-30 August 2013, 6 pp.

[6] C. Li, R. Burgos, I. Cvetkovic. D. Boroyevich, "Active and Reactive Power Flow Analysis of a STATCOM with Virtual Synchronous Machine Control, " in *Proc. of the 2015 IEEE 16th Workshop on Control and Modeling for Power Electronics*, Vancouver, British Columbia, Canada, 12-15 July 2015, 8 pp.

[7] J. Zhou, C. Booth, G. P. Adam, A. J. Roscoe, "Inertia Emulation Control of VSC-HVDC Transmission System," in *Proceedings of the 2011 International Conference on Advanced Power System Automation and Protection*, Beijing, China, 16-20 October 2011, 6 pp.

[8] J. Zhu, C. D. Booth, G. P. Adam, A. J. Roscoe, C. G. Bright, "Inertia Emulation Control Strategy for VSC-HVDC Transmission Systems" in *IEEE Transactions on Power Systems*, Vol. 28, No. 2, May 2013, pp. 1277-1287

[9] R. Aouini, B. Marinescu, K. B. Kilani, M. Elleuch, "Synchronverter-Based Emulation and Control of HVDC Transmission," in *IEEE Trans. on Power Systems*, Vol. 31, No. 1, January 2016, pp. 278-286

[10] M. Guan, W. Pan, J. Zhang, Q. Hao, J. Cheng, X. Zheng, "Synchronous Generator Emulation Control Strategy for Voltage Source Converter (VSC) Stations," in *IEEE Trans. Power Syst.*, Vol. 30, No. 6, Nov. 2016, pp. 3093-3101

[11] W. Zhang, K. Rouzbehi, J. I. Candela, A. Luna, P. Rodriguez, "Control of VSC-HVDC with Electromechanical Characteristics and Unified Primary Strategy," in *Proceedings of the 2016 IEEE Energy Conversion Congress and Exposition*, ECCE 2016, Milwaukee, Wisconsin, USA, 18-22 September 2016, 8 pp.

[12] E. Rakshani, D. Remon, A. M. Cantarellas, J. M. Garcia, P. Rodriguez, "Modeling and sensitivity analysis of VSP based virtual inertia controller in HVDC links of interconnected power systems," in *Electric Power System Research*, Vol. 141, Dec. 2016, pp. 246-263

[13] E. Rakhshani, P. Rodriguez, "Inertia Emulation in AC/DC Interconnected Power Systems Using Derivative Technique Considering Frequency Measurement Effects," in *IEEE Trans. Power Syst.*, Vol. 32, No. 5, Sept. 2017, pp.3338-3351

[14] H.-P. Beck, R. Hesse, "Virtual Synchronous Machine," in *Proceedings of the 9th International Conference on Electrical Power Quality and Utilisation*, Barcelona, Spain, 9-11 October 2007, 6 pp.

[15] S. D'Arco, J. A. Suul, Olav. B. Fosso, "A Virtual Synchronous Machine Implementation for Distributed Control of Power Converters in SmartGrids," in *Electric Power System Research*, Vol. 122, May 2015, pp. 180-197

[16] O. Mo, S. D'Arco, J. A. Suul, "Evaluation of Virtual Synchronous Machines with Dynamic or Quasi-stationary Machine Models," in *IEEE Trans. Ind. Electron.*, Vol. 64, No. 7, Jul. 2017, pp. 5952-5962

[17] J. Driesen, K. Visscher, "Virtual Synchronous Generators, *in Proceedings of the IEEE Power and Energy Society 2008 General Meeting: Conversion and Delivery of Energy in the 21st Century*, Pittsburgh, Pennsylvania, USA, 20-24 July 2008, 3 pp.

[18] K. Visscher, S. W. H. De Haan, "Virtual Synchronous Machines (VSG's) for Frequency Stabilization in Future Grids with a Significant Share of Decentralized Generation," in *CIRED seminar 2008: Smart Grids for Distribution*, Frankfurt, Germany, 23-24 June 2008, 4 pp.

[19] K. Sakimoto, Y. Miura, T. Ise, "Stabilization of a power system with a distributed generator by a virtual synchronous generator function," in *Proceedings of the 8th International Conference on Power Electronics – ECCE Asia*, Jeju, Korea, 30 May- 3 June 2011, 8 pp.

[20] Y. Hirase, K. Abe, K. Sugimoto, Y. Shindo, "A Grid-Connected Inverter with Virtual Synchronous Generator Model of Algebraic Type," in *El. Eng. in Japan*, vol. 184, no. 4, 2013, pp. 10-21, (*IEEJ Trans. on Power and Energy*, vol. 132, no. 4, pp. 371-380, April 2012

[21] Q.-C. Zhong, G. Weiss, "Synchronverters: Inverters That Mimic Synchronous Generators," *IEEE Trans. Ind. Electron.*, vol. 58, no. 4, pp. 1259-1267, Apr 2011

[22] S. D'Arco, J. A. Suul, "Virtual Synchronous Machines – Classification of Implementations and Analysis of Equivalence to Droop Controllers for Microgrids," in *Proceedings of IEEE PowerTech Grenoble 2013*, Grenoble, France, 16-20 June 2013, 7 pp.

[23] P. Kundur, "*Power System Stability and Control*," McGraw-Hill, 1994

[24] S. D'Arco, J. A. Suul, O. B. Fosso, "Automatic Tuning of Cascaded Controllers for Power Converters using Eigenvalue Parametric Sensitivities," in *IEEE Trans. on Industry Applications*, Vol. 51, No. 2, March/April 2015, pp. 1743-1753

[25] D. Duckwitz, B. Fisher, "Modeling and Design of df/dt-based Inertia Control for Power Converters," in *IEEE Journal of Emerging and Selected Topics in Power Electronics*, early access, 12 pp.

[26] S. D'Arco, J. A. Suul, and M. Molinas, "Implementation and analysis of a control scheme for damping of oscillations in VSC-based HVDC grids," in *Proc. 16th Int. Power Electronics and Motion Control Conf. and Expo.,* Antalya, Turkey, 21-24 September 2014, pp. 586–593.

[27] J. Z. Zhou, H. Ding, S. Fan, Y. Zhang, and A. M. Gole, "Impact of short-circuit ratio and phase-locked-loop parameters on the small-signal behavior of a VSC-HVDC converter," in *IEEE Transactions on Power Delivery*, Vol. 29, No. 5, October 2014, pp. 2287–2296

This is the accepted version of a paper published in Proceedings - 2018 IEEE 18th International Conference on Power Electronics and Motion Control - PEMC.
DOI: 10.1109/EPEPEMC.2018.8522010